

CUTTING TEMPERATURE MEASUREMENTS OF SEGMENTED CHIPS USING DUAL-SPECTRUM HIGH-SPEED MICROVIDEOGRAPHY

Jarred C. Heigel, Robert W. Ivester, and Eric P. Whinton
Manufacturing Engineering Laboratory
National Institute of Standards and Technology¹
Gaithersburg, Maryland

KEYWORDS

Chip Temperature Measurement, Orthogonal Cutting, Infrared Camera, Microvideography, Emissivity, Segmentation

ABSTRACT

Dual-spectrum high-speed microvideography involves the use of synchronized high-speed visible light and infrared cameras. This paper presents the application of such a system to determine chip temperatures during orthogonal cutting of American Iron and Steel Institute (AISI) 1045 steel with a coated carbide tool. Speeds from 200 m/min to 500 m/min and feeds of 0.15 mm/rev and 0.30 mm/rev represent industrially relevant cutting conditions². Obtaining temperature measurements at precise points of the chip by using the visible light images to navigate the infrared images proves to be advantageous.

INTRODUCTION

Numerous metal cutting research activities have been devoted towards understanding temperatures during metal cutting. Peak temperatures and their location along the rake face of the tool and in the chip indicate points of interest in the chip formation process and provide critical insight into key interactions among the tool, the chip, and the workpiece. These interactions drive important aspects of material removal, including tool wear, surface integrity, and residual stress formation (Taylor 1907; Tao and Lovell 2002). This information is critical for the design of new cutting processes and tools.

Researchers have measured tool temperature in several ways. Some researchers embedded thermocouples in cutting tools (Stephenson 1993; Stephenson and Agapiou 1994). Other researchers used the intrinsic (work-tool) thermocouple technique (Herbert 1926; Boston

¹ Commercial equipment and materials are identified in order to adequately specify certain procedures. In no case does such identification imply recommendation or endorsement by the National Institute of Standards and Technology, nor does it imply that the materials or equipment are necessarily the best available for the purpose. This paper is an official contribution of the National Institute of Standards and Technology and is not subject to copyright in the United States.

² 1 rev = 2π rad. The unit rev is widely used in the machining community as a result of the machine tool programming language.

and Gilbert 1935; Trigger 1948; Grzesik 1990; Stephenson 1993). Others have measured infrared spectrum emissions using single-point infrared pyrometers (Al Huda et al. 2002), and infrared cameras (Boothroyd 1961; Aluwihare et al. 2000; Davies et al. 2003; Davies et al. 2003) to estimate temperatures in an area of interest.

These methods have increased our understanding of the cutting process, but have limitations. Embedded thermocouples only measure the average temperature over the contact area at the junction between the thermocouple leads. This limits the spatial resolution to the size of the junction and the proximity to the location of interest (Roeser 1940). Intrinsic (work-tool) thermocouple systems must be calibrated according to the tool and workpiece materials as well as the tool-chip contact region. The extreme and varying contact conditions during metal cutting significantly limit the accuracy of the measurement. The temperature distribution over the tool-chip contact area generates a distribution of localized voltages leading to a single measurement voltage that is typically considered to represent the average of the temperature distribution. The precise relationship between the temperature distribution over the contact area and the single voltage measurement carries particular importance in metal cutting, where the temperature varies significantly over the contact area (Herbert 1926). Infrared imaging of orthogonal cutting provides a more detailed basis for understanding temperature distributions on the side of the tool during machining. However, the side of the cutting tool does not necessarily provide an accurate representation of the temperature distribution along the rake face of the tool-chip contact region. Furthermore, accurate determination of material emissivity limits the accuracy of infrared-based temperature measurements. Finally, cutting forces tend to deflect the tool, making it difficult to determine the tool boundaries in the infrared video.

High-speed visible light cameras used to study the metal cutting process have shown material flow and deformation patterns (Komanduri and Brown 1981; Ivester et al. 2007). Using a dual-spectrum system to simultaneously record visible light and infrared images at high frame rates during the metal cutting process reduces the measurement uncertainty of temperature measurement locations (Whitenton et al. 2005).

By calibrating the scale and location of the visible and infrared images, the visible light images define the tool boundaries in the infrared images. This paper presents the issues associated with directly correlating visible and infrared images, quantifies the temperature measurement uncertainties, and presents some results for orthogonal cutting of AISI 1045 steel.

EXPERIMENTAL SETUP

A modified grinding platform provides the test bed for orthogonal turning tests. The grinding platform allows a workpiece to be bolted to the spindle and lowered onto a stationary cutting tool. Workpieces range are 3.02 mm thick, 127 mm diameter discs cut from AISI 1045 cold-drawn steel rods (Ivester et al. 2007).

Commercially available Kennametal¹ A4G0605M06U4B KC5025 grooving inserts with a flat rake face, held in a A4SML160624 tool holder attached to the face of a 3-axis Kistler¹ dynamometer provide the orthogonal cutting edge for the experiments. The tool holder provides a clearance angle of 7° and a rake angle of 5°. Testing conditions of 0.15 mm/rev and 0.30 mm/rev feed rate and 200 m/min to 500 m/min cutting speed represent industrially relevant cutting conditions. Careful positioning of the cutting tool places the side of the chip at the edge of the ground side surface of the tool.

Figure 1 shows the experimental setup. A digital oscilloscope records the dynamometer signals at a sampling rate of 2 MHz before down sampling to 500 Hz for analysis. A high speed

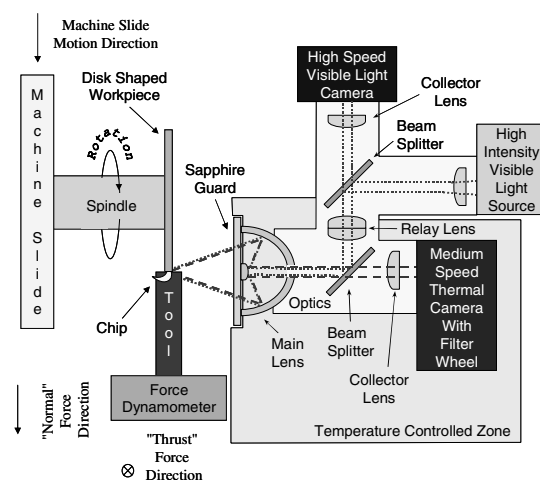


FIGURE 1. DUAL SPECTRUM SETUP.

visible light camera (shutter speed of 30 000 frames per second (fps), integration time of 33 s) and a medium speed infrared camera (600 fps shutter speed, 10 μ s to 25 μ s integration time, 3 m to 5 m wavelength) simultaneously record the cutting process. The disk-shaped workpiece rotates on the horizontal spindle and moves on a vertical axis (feed direction). The slide holding the cutting tool and dynamometer does not move during the tests, so the cameras can be mounted on a high-stiffness metrology stand on the floor to reduce the effect of machine tool vibrations on the camera setup. Synchronizing the dynamometer, visible light camera, and infrared camera signals by reading each signal with an oscilloscope at 2 MHz sampling rate provides confidence the signals represent nearly identical instances in time.

Image Calibration

Taking pictures of a standard grid pattern with known dot spacing using both cameras provides the means to calibrate the scaling of the visible image and to register the infrared image to the visible image. Figure 2 shows the two images overlapped after the registering process. Scaling dots are spaced 0.1 mm apart.

Chip Emissivity

Post-process analysis of the chips was used to determine the chip emissivity. This process involves imaging several different chips heated to an assortment of uniform steady state temperatures. A horizontal filter simulates the effect of motion blur to better represent the chip formation measurement. Comparing the temperature of the chip measured with a

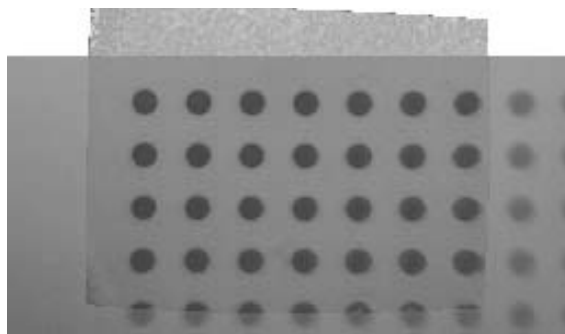


FIGURE 2. VISIBLE GRID IMAGE AND REGISTERED INFRARED GRID IMAGE.

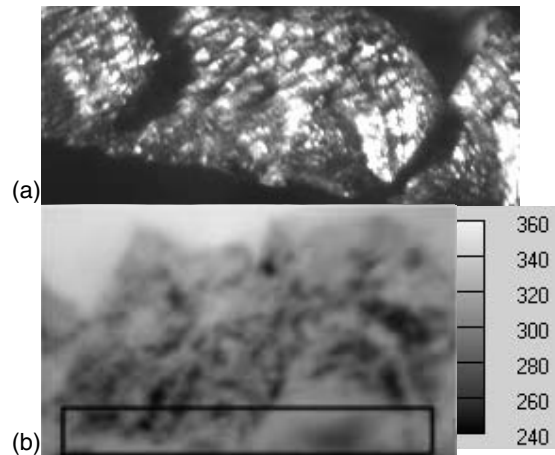


FIGURE 3. IMAGES OF POST PROCESS CHIP. A) VISIBLE, B) THERMAL INDICATING ANALYSIS REGION, SCALE IN RADIANCE °C.

thermocouple to its apparent average radiance temperature over a selected area of the chip provides an estimate of emissivity. Figure 3 illustrates visible and infrared images of a chip at 369 °C, measured using a thermocouple. The chip is approximately 0.5 mm high. This analysis results in a chip emissivity of 0.45 +/- 0.09 with a k=1 coverage factor. The relatively large emissivity uncertainty (+/- 20%) results from the non-uniformity of the chip surface as seen in Figure 3. Steady state and uniform temperature is ensured by providing sufficient time to heat and maintain the chip at a given temperature. Considering the temperature is constant across the surface, the radiance temperature readings in Figure 3 range from 240 °C radiance to approximately 320 °C radiance in the selected surface area of the chip.

The oxide-layer on the chip affects chip emissivity. Oxide layer formation is different during machining than it is during post-process measurements. During machining the chip surface deforms significantly and the surface temperature leads to the build-up of an oxide layer that affects the emissivity of the chip surface in a way that is difficult to measure. The emissivity value of 0.45 was determined based on post-process measurements of chips showing a lesser oxide layer because these better represent the condition of the chip during the cutting process.

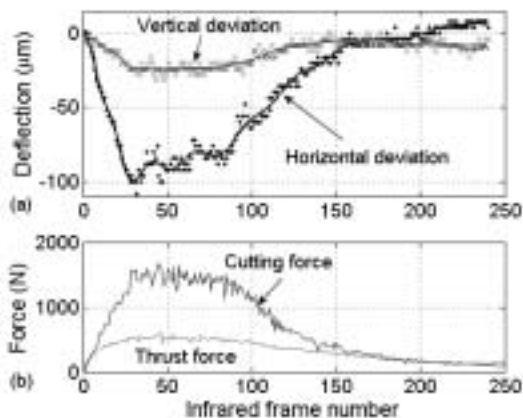


FIGURE 4. 400 m/min 0.30 mm/rev A) DEFLECTION, B) FORCES

Tool Tracking

Using the tool tip as a reference point in the video frames enables tracking the location of various points of interest. Because the experimental setup compromises the tool holding stiffness, the tool must be tracked during the test. Figure 4 illustrates the typical amount of tool movement and experimental force for one test. Matlab¹ code tracks the tool by creating a dataset of manually selected horizontal and vertical tool tip pixel coordinates in the visible light frame for each infrared video frame. The fluctuation of shadows caused by chips obstructing different light sources throughout the test necessitates smoothing the data with a polynomial fit. The stiffness appears lower than expected for the commercially supplied tool holder. The cameras are mounted on the floor outside of the machine tool, so several factors could account for this lower stiffness, including (1) the cantilevered tool, (2) the dynamometer, (3) the rotary table and linear axis under the dynamometer. The observed deflection rate does not affect the relative speed of the incoming uncut workpiece material. Figure 4 illustrates that during steady state machining (between frames 50 and 80) the vertical deflection is relatively small. Because several revolutions of the workpiece are made during this time, the deflection does not affect the feed.

ANALYSIS METHODOLOGY

The measurands implemented to study chip temperature include average peak chip temperature during steady state, average chip rake face temperature during steady state, and

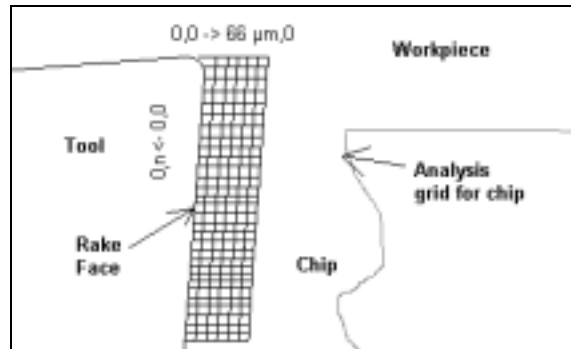


FIGURE 5. GRID PATTERN USED FOR CHIP TEMPERATURE ANALYSIS.

steady state temperature distribution. All these measurands were obtained by applying an analysis grid to the chip projecting from the insert rake face (Figure 5). This approach allows the temperature values in each grid square to be averaged together, smoothing the data and minimizing noise effects. Grid section dimensions of 3 x 3 pixels maintain adequate analysis resolution. The camera's minimum measurable temperature (a result of integration rate) artificially inflates the average chip temperature value over the entire chip area because temperatures below the minimum value are ignored. To eliminate this effect, the chosen grid area contains temperatures consistently above the minimum in all observed tests.

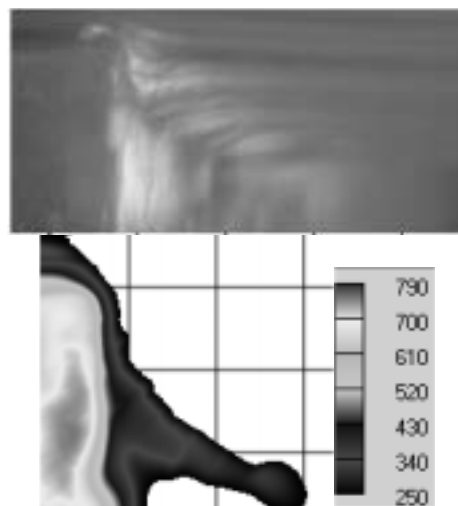


FIGURE 6. VISIBLE AND INFRARED IMAGES OF METAL CUTTING AT 400 m/min, 0.30 mm/rev. TEMPERATURE SCALE IN RADIANCE °C.

RESULTS

Figure 6 shows typical visible and infrared frames obtained during an experiment. The infrared image shows a newly-formed segment boundary, and represents the segmented chip formation that occurred in all of the tests. Table 1 presents the forces, average peak chip temperatures during steady state cutting, and average chip rake face temperatures during steady state cutting. Figure 7 plots chip temperatures against specific thrust forces. The Appendix contains figures illustrating cutting forces and peak temperatures with respect to time and the average temperature distribution on the chip surface during steady state. Dotted vertical lines represent the beginning and end of steady state. In the latter plots, each curve represents a column of analysis grid sections at different distances away from the rake face.

The plots in Figure 7 show the linear behavior of the peak chip temperature obtained during this investigation. When plotted against surface speed (Figure 7a), the peak temperature increases dependant upon the feed rate, where the peak temperatures measured for the 0.15 mm/rev feed tests are consistently less than the 0.3 mm/rev feed tests. However, dependence on feed appears irrelevant when comparing the peak temperature to the specific forces (Figure 7b and Figure 7c).

Care should be taken when comparing the results herein with those of continuous chip formation. Prior work (Komanduri and Hou 2002, Ivester et al. 2007) has shown that segmentation events involve a localized shear zone which is rolled onto the rake surface of the tool. While on

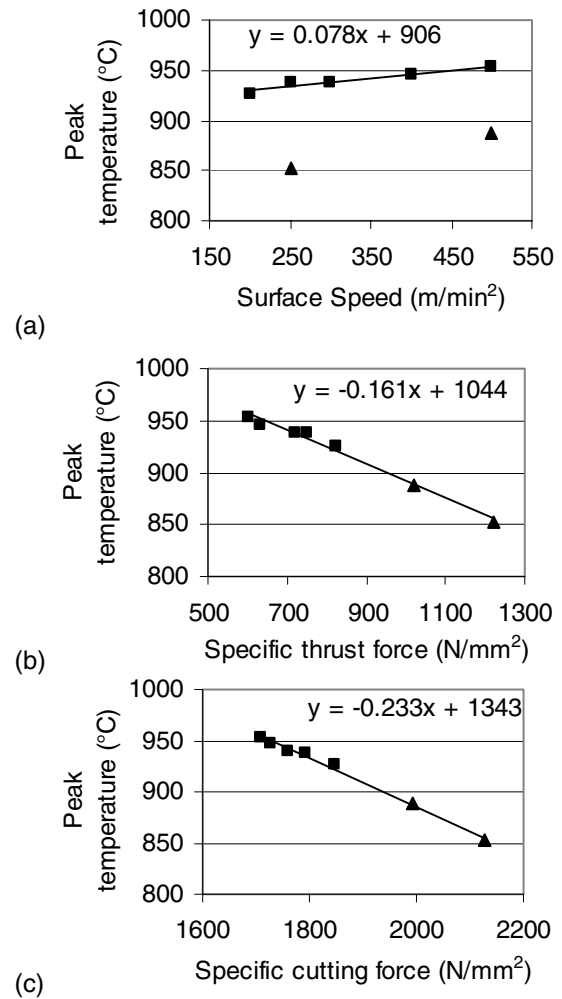


FIGURE 7. PEAK CHIP TEMPERATURE DURING STEADY STATE VS. A) SURFACE SPEED, B) SPECIFIC THRUST FORCE, C) SPECIFIC CUTTING FORCE. TRIANGLE SYMBOLS REPRESENT 0.15 mm/rev, SQUARE SYMBOLS REPRESENT 0.30 mm/rev.

TABLE 1. FORCE, CHIP PEAK TEMPERATURE, AND AVERAGE RAKE FACE TEMPERATURE, ALL MEASURED DURING STEADY STATE ORTHOGONAL CUTTING.

Cutting Conditions		Specific Forces		Chip Temperature	
Feed mm/rev	Speed m/min	Thrust (N/mm ²)	Cutting (N/mm ²)	Peak during steady state (°C)	Average chip rake face (°C)
0.15	250	1223 ± 59	2126 ± 72	852 ± 116	720 ± 217
0.15	500	1020 ± 40	1992 ± 72	888 ± 156	652 ± 272
0.3	200	823 ± 47	1846 ± 53	926 ± 169	749 ± 253
0.3	250	751 ± 34	1794 ± 47	938 ± 171	700 ± 303
0.3	300	718 ± 28	1759 ± 46	939 ± 186	713 ± 261
0.3	400	631 ± 17	1727 ± 45	946 ± 155	765 ± 262
0.3	500	603 ± 25	1709 ± 42	953 ± 142	770 ± 268

the rake surface, the material remains stationary until the current segment is ruptured from the workpiece by a new shear localization event. Since the shear localization significantly preheats the material prior to contacting the rake surface, the rake friction and temperature during the formation of a segmented chip may be different than a continuous chip.

CONCLUSION

This paper presented experimental results using high-speed microvideography with synchronized high speed visible light (30 000 fps) and infrared (600 fps) cameras. These results include temperature measurements of segmented chips during orthogonal cutting of AISI 1045 steel with a coated carbide tool. The cutting conditions for these experiments represent industrially relevant conditions, 200 m/min to 500 m/min cutting speeds and 0.15 mm/rev and 0.30 mm/rev feed rates. The analysis method using the visible light images to navigate the infrared images leads to improved measurements of segmented chip temperatures. The resulting average chip rake face temperature measurements during steady state cutting ranged from 652 °C to 770 °C, and the average peak chip temperature measurements during steady state cutting ranged from 852 °C to 953 °C. The emissivity of the chip surface formed the dominant component of the measurement uncertainty in all tests.

REFERENCES

- Al Huda, M., K. Yamada, et al. (2002). "Investigation of Temperature at Tool-Chip Interface in Turning Using Two-Color Pyrometer." *Journal of Manufacturing Science and Engineering, Transactions of the ASME*, Vol. 124, Num. 2, pp. 200-207.
- Aluwihare, C.B., E.J.A. Armarego, et al. (2000). "A Predictive Model for Temperature Distributions in 'Classical' Orthogonal Cutting." *Transactions of the North American Manufacturing Research Institution of SME*, Vol. 28, Num. 1, pp. 131-136.
- Boothroyd, G. (1961). "Photographic Technique for the Determination of Metal Cutting Temperatures." *British Journal of Applied Physics*, Vol. 12, Num. 1, pp. 238-242.
- Boston, O.W. and W.W. Gilbert (1935). "Cutting Temperatures Developed by Single-Point Turning Tools." *Transactions of the ASM*, Vol. 23, Num. 1, pp. 703-726.
- Davies, M.A., Q. Cau, et al. (2003). "On the Measurement and Prediction of Temperature Fields in Machining AISI 1045 Steel." *CIRP Annals - Manufacturing Technology*, Vol. 52(1), pp. 77-80.
- Davies, M.A., H. Yoon, et al. (2003). "Calibrated Thermal Microscopy of the Tool-Chip Interface in Machining." *Machining Science and Technology*, Vol. 7, Num. 2, pp. 167-190.
- Grzesik, W. (1990). "The Mechanics of Continuous Chip Formation in Oblique Cutting with Single-Edged Tool. 2. Experimental-Verification of the Theory." *International Journal of Machine Tools & Manufacture*, Vol. 30, Num. 3, pp. 373-388.
- Herbert, E.G. (1926). "The Measurement of Cutting Temperatures." *Proceedings of the Institute of Mechanical Engineers*, pp. 289-329.
- Ivester, R.W., E. Whitenon, et al. (2007). "Measuring Chip Segmentation by High-Speed Microvideography and Comparison to Finite-Element Modeling Simulations." *10th International Workshop on Modeling of Machining Operations*, Calabria, Italy, CIRP.
- Komanduri, R., Brown, R.H., (1981). "On the Mechanics of Chip Segmentation in Machining." *Journal of Engineering for Industry*, Vol. 103, pp. 33-51.
- Komanduri, R., Hou, Z.-B., (2002). "On Thermoplastic Shear Instability in the Machining of a Titanium Alloy (Ti-6Al-4V)." *Metallurgical and Materials Transactions A*, Vol. 33A, pp. 2995-3010.
- Roeser, W.F., (1940). "Thermoelectric Thermometry." *Journal of Applied Physics*, Vol. 11, pp. 388-407.
- Stephenson, D.A. (1993). "Tool-Work Thermocouple Temperature Measurements-Theory and Implementation Issues." *Journal of Engineering for Industry-Transactions of the ASME*, Vol. 115, Num. 4, pp. 432-437.
- Stephenson, D.A. and J.S. Agapiou (1994). *Metal Cutting Theory and Practice*, New York, NY, Marcel Dekker.

Tao, Z. and M.R. Lovell (2002). "Towards an Improved Friction Model in Material Removal Processes: Investigating the Role of Temperature." *Transactions of the North American Manufacturing Research Institution of SME*, Vol. 30, Num. 1, pp. 493-500.

Taylor, B.N. and C.E. Kuyatt (1994). "Guidelines for Evaluating and Expressing the Uncertainty of NIST Measurement Results." NIST TN 1297.

Taylor, F.W. (1907). "On the Art of Cutting Metals." *Transactions of the ASME*, Vol. 28, pp. 31-350.

Trigger, K.J. (1948). "Progress Report No. 1 on Tool-Chip Interface Temperatures." *Transactions of the ASME*, Vol. 70: pp. 91-98.

Whitenton, E., R.W. Ivester, et al. (2005). "Simultaneous Visible and Thermal Imaging of Metals During Machining." Thermosense XXVII, Orlando, FL, International Society for Optical Engineering.

APPENDIX

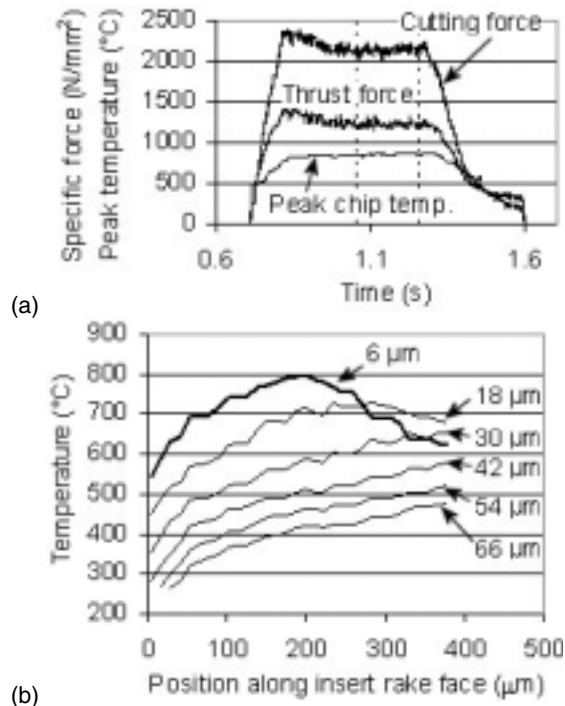


FIGURE 8. 250 m/min., 0.15 mm/rev. (a) TEST DATA, (b) CHIP TEMPERATURE DISTRIBUTION.

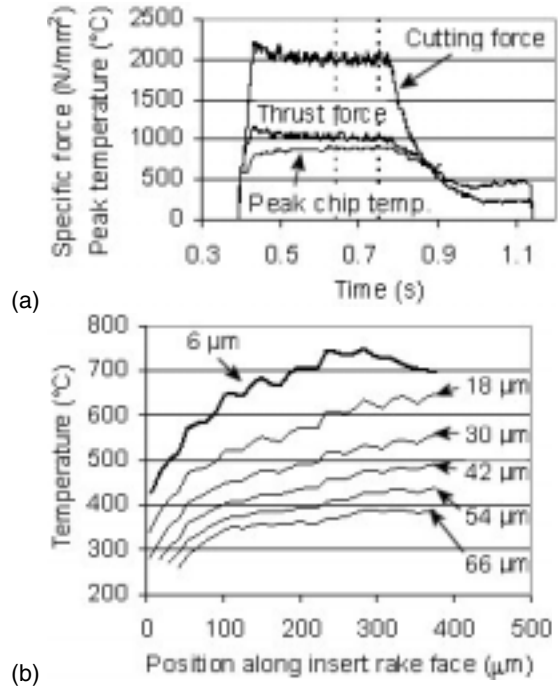


FIGURE 9. 500 m/min., 0.15 mm/rev. (a) TEST DATA, (b) CHIP TEMPERATURE DISTRIBUTION.

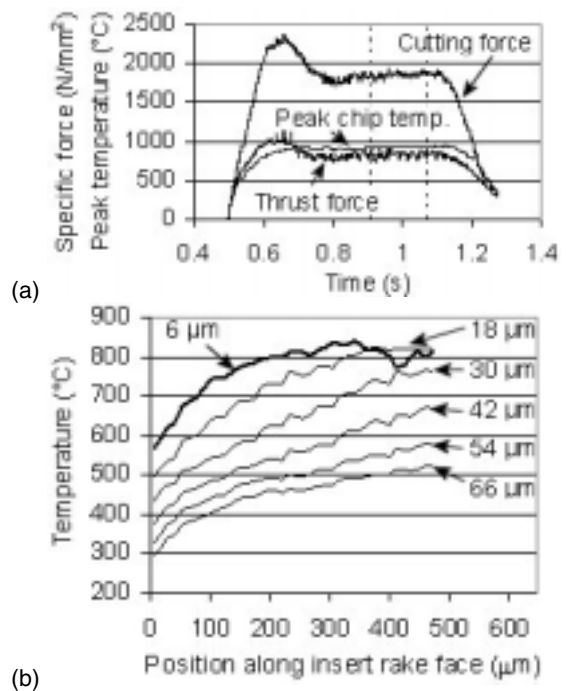


FIGURE 10. 200 m/min., 0.30 mm/rev. (a) TEST DATA, (b) CHIP TEMPERATURE DISTRIBUTION.

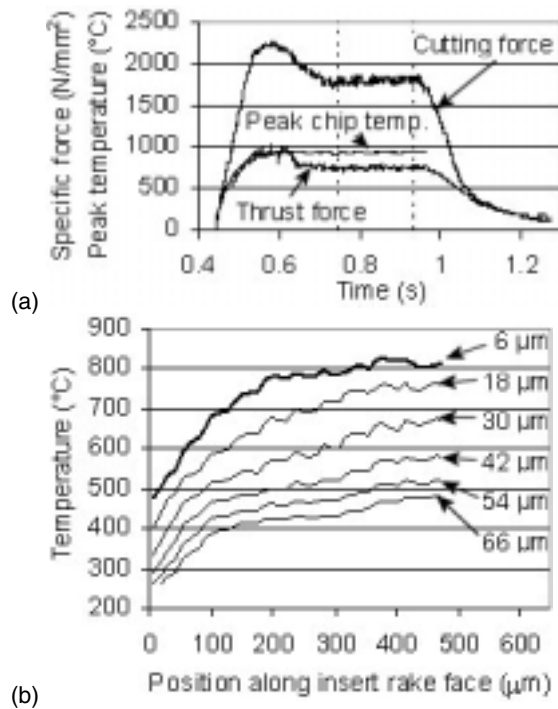


FIGURE 11. 250 m/min., 0.30 mm/rev. (a) TEST DATA, (b) CHIP TEMPERATURE DISTRIBUTION.

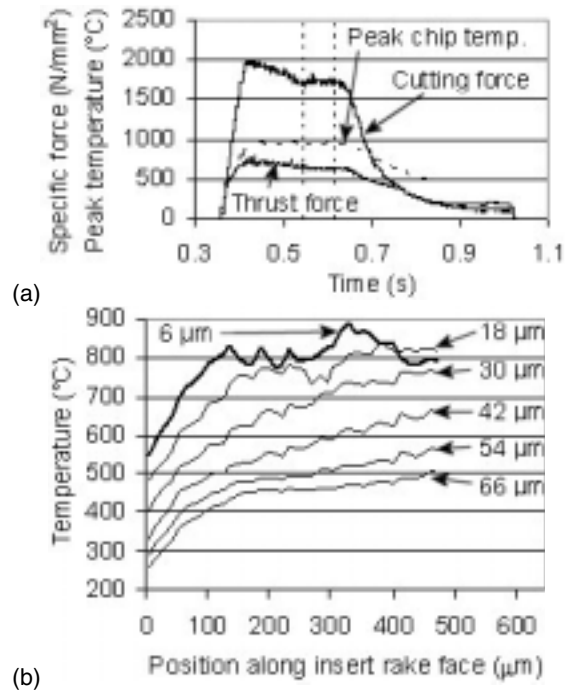


FIGURE 13. 400 m/min., 0.30 mm/rev. (a) TEST DATA, (b) CHIP TEMPERATURE DISTRIBUTION.

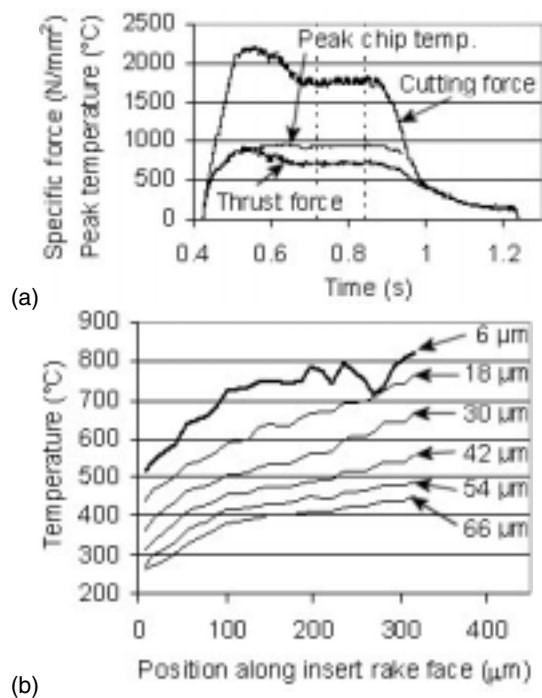


FIGURE 12. 300 m/min., 0.30 mm/rev. (a) TEST DATA, (b) CHIP TEMPERATURE DISTRIBUTION.

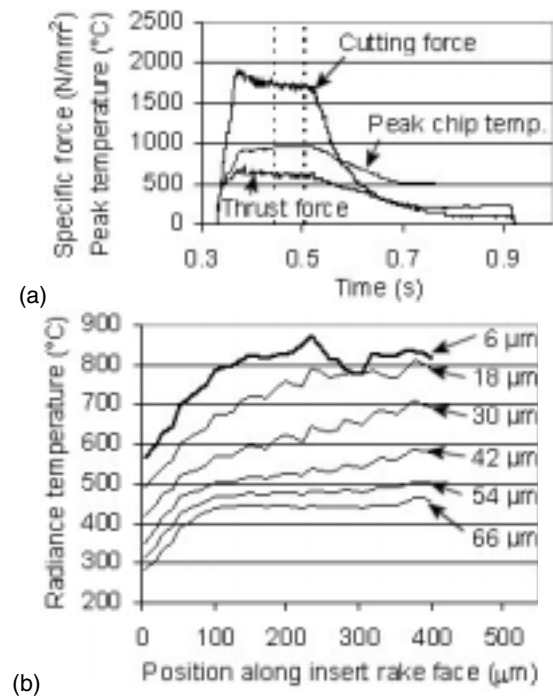


FIGURE 14. 500 m/min., 0.30 mm/rev. (a) TEST DATA, (b) CHIP TEMPERATURE DISTRIBUTION.